Ultra-broadband terahertz perfect absorber by exciting multi-order diffractions in a double-layered grating structure

Yan Peng, XiaoFei Zang,* YiMing Zhu, Cheng Shi, Lin Chen, Bin Cai, and SongLin Zhuang

Shanghai Key Lab of Modern Optical System, and University of Shanghai for Science and Technology, No.516 JunGong Road, Shanghai 200093, China

** xfzang@usst.edu.cn*

Abstract: Terahertz (THz) perfect absorber, as a useful functional device, has attracted considerable attention. Traditional metamaterial perfect absorbers are usually in response to single-frequency or multi-frequency owing to the resonance features of the metal-based sub-wavelength structure. In this paper, a simple double-layered doped-silicon grating structure was designed to realize an ultra-broadband and polarization-independent THz perfect absorber. Both theoretical and experimental results demonstrate that the incident THz waves ranging from 0.59 to 2.58 THz can be efficiently absorbed with an absorptivity of more than 95% and a bandwidth of about 2.0 THz. The excellent characteristic of this broad-bandwidth THz perfect absorber is mainly resulted from the air gap mode resonance together with the first-order and the second-order grating diffractions.

OCIS codes: (050.6624) Subwavelength structures; (300.6495) Spectroscopy, terahertz; (310.3915) Metallic, opaque, and absorbing coatings.

References and links

1. X. Liu, T. Starr, A. F. Starr, and W. J. Padilla, "Infrared spatial and frequency selective metamaterial with near-Unity absorbance," Phys. Rev. Lett. **104**(20), 207403 (2010).
2. N. Liu, M. Mesch, T. Weiss, M. Hentschel, and H. Giessen, "Infrared perfect absorber and its application as plasmonic sensor," Nano Lett. **10**(7), 2342–2348 (2010).
3. F. Alves, D. Grbovic, B. Kearney, N. V. Lavrik, and G. Karunasiri, "Bi-material terahertz sensors using metamaterial structures," Opt. Express **21**(11), 13256–13271 (2013).
4. N. I. Landy, S. Sajuyigbe, J. J. Mock, D. R. Smith, and W. J. Padilla, "Perfect metamaterial absorber," Phys. Rev. Lett. **100**(20), 207402 (2008).
5. H.-T. Chen, J. F. Zhou, J. F. O'Hara, F. Chen, A. K. Azad, and A. J. Taylor, "Antireflection coating using metamaterials and identification of its mechanism," Phys. Rev. Lett. **105**(7), 073901 (2010).
6. H. Tao, N. I. Landy, C. M. Bingham, X. Zhang, R. D. Averitt, and W. J. Padilla, "A metamaterial absorber for the terahertz regime: design, fabrication and characterization," Opt. Express **16**(10), 7181–7188 (2008).
7. H. Tao, C. M. Bingham, A. C. Strikwerda, D. Pilon, D. Shrekenhamer, N. I. Landy, K. Fan, X. Zhang, W. J. Padilla, and R. D. Averitt, "Highly flexible wide angle of incidence terahertz metamaterial absorber: design, fabrication, and characterization," Phys. Rev. B **78**(24), 241103 (2008).
8. Y. Q. Ye, Y. Jin, and S. L. He, "Omnidirectional, polarization-insensitive and broadband thin absorber in terahertz regimem," J. Opt. Soc. Am. B **27**(3), 498–504 (2010).
9. Y. Ma, Q. Chen, J. Grant, S. C. Saha, A. Khalid, and D. R. Cumming, "A terahertz polarization insensitive dual band metamaterial absorber," Opt. Lett. **36**(6), 945–947 (2011).
10. H.-T. Chen, "Interference theory of metamaterial perfect absorbers," Opt. Express **20**(7), 7165–7172 (2012).
11. X. Y. Peng, B. Wang, S. Lai, D. H. Zhang, and J. H. Teng, "Ultrathin multi-band planar metamaterial absorber based on standing wave resonances," Opt. Express **20**(25), 27756–27765 (2012).
12. L. Huang, D. R. Chowdhury, S. Ramani, M. T. Reiten, S. N. Luo, A. J. Taylor, and H.-T. Chen, "Experimental demonstration of terahertz metamaterial absorbers with a broad and flat high absorption band," Opt. Lett. **37**(2), 154–156 (2012).

#226580 - $15.00 USD Received 10 Nov 2014; revised 1 Jan 2015; accepted 20 Jan 2015; published 26 Jan 2015

13. L. Huang, R. D. Chowdhury, S. Ramani, M. T. Reiten, S. N. Luo, A. K. Azad, A. J. Taylor, and H.-T. Chen, "Impact resonator geometry and its coupling with ground plane on ultrathin metamaterial perfect absorbers," Appl. Phys. Lett. **101**(10), 101102 (2012).
14. J. Zhu, Z. Ma, W. Sun, F. Ding, Q. He, L. Zhou, and Y. Ma, "Ultra-broadband terahertz metamaterial absorber," Appl. Phys. Lett. **105**(2), 021102 (2014).
15. X. P. Shen, Y. Yang, Y. Zang, J. Gu, J. Han, W. Zhang, and T. J. Cui, "Triple-band terahertz metamaterial absorber: design, experiment, and physical interpretation," Appl. Phys. Lett. **101**(15), 154102 (2012).
16. W. Zhu and X. Zhao, "Metamaterial absorber with dendritic cells at infrared frequencies," J. Opt. Soc. Am. B **26**(12), 2382–2385 (2009).
17. X. P. Shen, T. J. Cui, J. Zhao, H. F. Ma, W. X. Jiang, and H. Li, "Polarization-independent wide-angle triple-band metamaterial absorber," Opt. Express **19**(10), 9401–9407 (2011).
18. Y. Chen, J. Dai, M. Yan, and M. Qiu, "Honeycomb-lattice plasmonic absorbers at NIR: anomalous high-order resonance," Opt. Express **21**(18), 20873–20879 (2013).
19. D. Shrekenhamer, W.-C. Chen, and W. J. Padilla, "Liquid crystal tunable metamaterial absorber," Phys. Rev. Lett. **110**(17), 177403 (2013).
20. H. R. Seren, G. R. Keiser, L. Cao, J. Zhang, A. C. Strikwerda, K. Fan, G. D. Metcalfe, M. Wraback, X. Zhang, and R. D. Averitt, "Optically modulated multiband terahertz perfect absorber," Adv. Opt. Mater. **2**(12), 1221–1226 (2014).
21. J. Sun, L. Liu, G. Dong, and J. Zhou, "An extremely broad band metamaterial absorber based on destructive interference," Opt. Express **19**(22), 21155–21162 (2011).
22. Y. X. Cui, K. H. Fung, J. Xu, H. Ma, Y. Jin, S. He, and N. X. Fang, "Ultrabroadband light absorption by a sawtooth anisotropic metamaterial slab," Nano Lett. **12**(3), 1443–1447 (2012).
23. D. Ye, Z. Wang, K. Xu, H. Li, J. Huangfu, Z. Wang, and L. Ran, "Ultrawideband dispersion control of a metamaterial surface for perfectly-matched-layer-like absorption," Phys. Rev. Lett. **111**(18), 187402 (2013).
24. W. Li, T. Wu, W. Wang, J. Guan, and P. Zhai, "Integrating non-planar metamaterials with magnetic absorbing materials to yield ultra-broadband microwave hybrid absorbers," Appl. Phys. Lett. **104**(2), 022903 (2014).
25. R. Kakimi, M. Fujita, M. Nagai, M. Ashida, and T. Nagatsuma, "Capture of a terahertz wave in a photonic crystal slab," Nat. Photonics **8**(8), 657–663 (2014).
26. M. Pu, M. Wang, C. Hu, C. Huang, Z. Zhao, Y. Wang, and X. Luo, "Engineering heavily doped silicon for broadband absorber in the terahertz regime," Opt. Express **20**(23), 25513–25519 (2012).
27. C. Shi, X. F. Zang, Y. Q. Wang, L. Chen, and Y. M. Zhu, "A polarization-independent broadband terahertz absorber," Appl. Phys. Lett. **105**(3), 031104 (2014).

1. Introduction

In the past few years, perfect absorber as one of the most exciting issues has aroused great interest due to its wide applications in spectrum imaging system, sensor, thermal emitter and so on [1–3]. Based on metamaterial technology, Landy et. al., proposed the first perfect absorber in micro-wave regime [4]. In their work, a splitting ring resonator (SRR)/loss dielectric spacer/metal-wire sandwich 'fishnet' structure was designed to couple electric and magnetic fields, separately, leading to a single-frequency and polarization-dependent perfect absorber. Subsequently, another sandwich structure consisting of a symmetrical metal-based electric ring resonator (ERR), loss dielectric spacer, and a metal mirror substrate was proposed to realize the polarization-independent single-frequency perfect absorber [5]. By adding more ERR with different sizes or shapes in an absorption unit cell, dual-band, triple-band, and multi-band perfect absorbers were also demonstrated in microwave, THz, and optical regimes [6–18]. Tunable perfect absorber, as a research hotspot, has also attracted much attention [19, 20]. Broadband perfect absorber, as a pursuit goal of many researchers, can be obtained by introducing multi-layered (much more than two layers) gradually varied ERR structure [21–24]. All of the resonance absorption peaks induced by multi-layered gradually varied ERR are close to each other, thereby forming a broadband perfect absorber. Although wideband perfect absorber has been verified by virtual of multi-layered gradually varied ERR structure, it is suffering from the difficulties of either alignment or fabrication, leading to the impracticality in practical application. Therefore, the development of a simple structured broadband perfect absorber is one critical problem that needs to be solved urgently.

In order to realize such a broadband perfect absorber with simple structure, a semiconductor photonic-crystal, which can be fabricated by etching periodical air pillars in a doped-silicon slab, was proposed by R. Kakimi et. al. It can capture THz waves with high efficiency and broad-bandwidth [25]. By optimizing the lattice parameters, the guided-mode

#226580 - $15.00 USD Received 10 Nov 2014; revised 1 Jan 2015; accepted 20 Jan 2015; published 26 Jan 2015

resonance and the Fabry–Pérot resonance (by introducing a metal mirror underneath the photonic-crystal slab), can be combined with each other, obtaining a THz absorber with the bandwidth of 50 GHz (absorptivity≥90%). In addition, a doped silicon-based grating array was theoretically reported by M. Pu et. al., and was experimentally verified by our previous work [26, 27]. This kind of broadband THz absorbers were realized based on the destructive interference (antireflection effects) and the first-order grating diffraction. According to the above logic, one may ask that is it possible to broaden the absorption bandwidth by exciting high-order grating diffraction?

In this paper, motivated by the above problem, a double-layered doped silicon grating array was fabricated to excite the second-order grating diffraction. Different from the exciting of guide-mode resonance and the Fabry–Pérot resonance in Ref [25], our double-layered grating array is proposed to excite the air-gap mode resonance, the first-order grating diffraction, and the second-order grating diffraction. By optimizing the doping density, the air gap mode resonance (non-antireflection effects), and the first- and second-order grating diffractions can be broadened and then merge with each other, resulting in an ultra-broadband THz absorber with an absorptivity of 95% and a bandwidth of about 2 THz. To the best of our knowledge, such an absorption bandwidth obtained in this study is much broader than that of the previously reported THz absorbers.

2. Results and discussion

The schematic of ultra-broadband THz absorber is shown in Figs. 1(a) and 1(b), respectively. It is a typical three-layered structure consisting of double-layered grating structure and substrate. The double-layered gratings structure is composed of periodical square pillars, but with different widths. In Figs. 1(a) and 1(b), each of the unit cells has a square lattice with 90 degree rotational symmetry, which means that our THz absorber is insensitive to the polarization of the incident THz wave. In this paper, both the double-layered grating and the substrate are consisting of boron-doped silicon with resistivity of 0.54 Ω·cm, and the corresponding permittivity can be written as follows:

$$\varepsilon = \varepsilon_{\infty} - \frac{\omega_p^2}{\omega(\omega + i/\tau)}, \tag{1}$$

where $\varepsilon_{\infty} = 11.7$, $\tau = 0.571$ ps is the carrier relaxation time and $\omega_p = 19.1$ THz is the plasmon frequency. The detailed geometry parameters of this ultra-broadband THz absorber are p = 100 μm, a_1 = 80 μm, and a_2 = 45 μm. The heights of the double-layered grating and the substrate are $h_{grating}$ = 40μm ($h_1 = h_2$ = 40μm) and $h_{substrate}$ = 420μm, respectively.

#226580 - $15.00 USD Received 10 Nov 2014; revised 1 Jan 2015; accepted 20 Jan 2015; published 26 Jan 2015

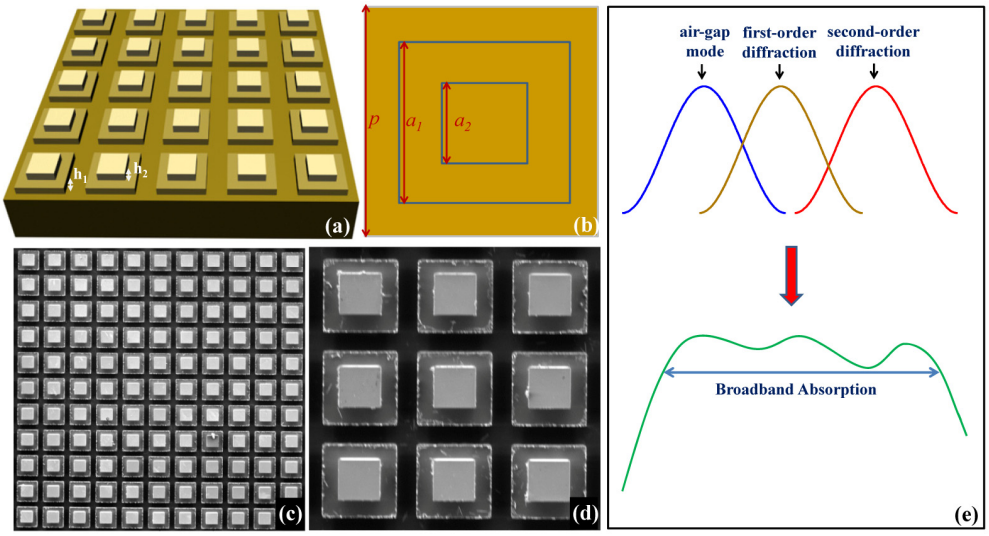

Fig. 1. Configuration and principle of the broadband THz absorber. (a) and (b) Schematic diagram of the sample. (c) and (d) SEM of the fabricated sample. (e)The fundamental principle of the ultra-broadband THz absorber

Figures 1(c) and 1(d) depict the scanning electron microscope (SEM) images of the double-layered doped-silicon grating structure. The fabrication process consists of two parts: the traditional photolithography and the inductively coupled plasma (ICP) etching on a 0.54 Ω·cm *p*-type silicon wafer (with thickness of 500 μm). First, a 1 μm AZP4620 image reversal photoresist layer was spin-coated on the doped-silicon substrate. The first-layer of grating is patterned based on the standard photolithography. By etching for a proper time, the first-layer of grating with height h = 80 μm and width a_1 = 80 μm is formed on the surface of the doped silicon. By repeating the above steps, the second-layer of grating with height h = 40 μm and width a_2 = 45 μm can also be formed by etching the first-layered grating. Figure 1(e) shows the fundamental principle (the idea of the wave trapping) of our designed ultra-broadband THz absorber. These three peaks in Fig. 1(e) (the upper image) are corresponding to the air-gap mode resonance, the first-order grating diffraction, and the second-order grating diffraction, respectively. The air-gap mode resonance is excited by the bottom grating array, while both the first-order grating diffraction and the second-order grating diffraction are excited by the double-layered grating array. In our paper, the carrier density is $N = 1.6 \times 10^{16}$ cm^{-3} (with the resistivity of 0.54 Ω·cm), and thereby such a heavily doped silicon-based grating structure have metallic characteristic. In this case, the imaginary component of the index is very large (For example, at f = 1.294 THz, the index of the heavily doped silicon is n = 3.28 + 0.33i). Therefore, when the incident THz waves resonated with the high loss doped-silicon grating, these resonance peaks are broadened. For example, at f = 1.294 THz, the peak induced mainly by the first-order grating diffraction can be broadened in such relatively low Q-factor (Q = 8.25) silicon-based grating structure [see the inset in Fig. 2(a)]. Similarly, the other two peaks at f = 0.789 THz, and f = 2.083 THz can also be broadened. As a result, the doped-silicon grating array can reduce the quality-factor at these three resonance frequencies, and then these three resonance peaks are broadened and thus overlapped with each other as shown in Fig. 1(e) (the bottom image), resulting in the broadband wave trapping.

Figures 2(a) and 2(b) show the calculated results of this ultra-broadband THz absorber. For TE (transverse electric) THz wave, as shown in Fig. 2(a), the incident THz waves ranging from 0.59 to 2.58 THz can be efficiently absorbed with the absorption efficiency of more than 95%, and the absorption bandwidth is nearly about 2 THz. For TM (transverse magnetic) THz wave, the absorption spectrum shown in Fig. 2(b) is the same as that in Fig. 2(a), which

#226580 - $15.00 USD Received 10 Nov 2014; revised 1 Jan 2015; accepted 20 Jan 2015; published 26 Jan 2015

means that our THz absorber is polarization-independent of the incident THz waves. To measure the absorbance characterizes of this THz absorber, THz time-domain spectroscopy (THz-TDS) system ranging from 0.2 THz to 2.8 THz with a 4.85 GHz spectral resolution is used to measure the transmission and reflectance spectra. The absorption efficiency is characterized as $A = 1\text{-}R\text{-}T$, where A is absorptivity, R is the reflectivity and T is the transmissivity. The corresponding results are presented in Figs. 2(c) and 2(d), where the absorption efficiency is over 95% with bandwidth more than 2 THz for both TE and TM incident waves. By comparing Figs. 2(a) and 2(c) [or Figs. 2(b) and 2(d)], we can also find that the measured spectra agree well with the calculated spectra, except for a slight discrepancy in the resonant frequency. This can be attributed to the difference between the calculated models and the fabricated structure. Additionally, all of them have three peaks in the absorption spectra. Therefore, such an ultra-broadband THz absorber is closely linked with these three peaks, as labeled by three arrows in Fig. 2.

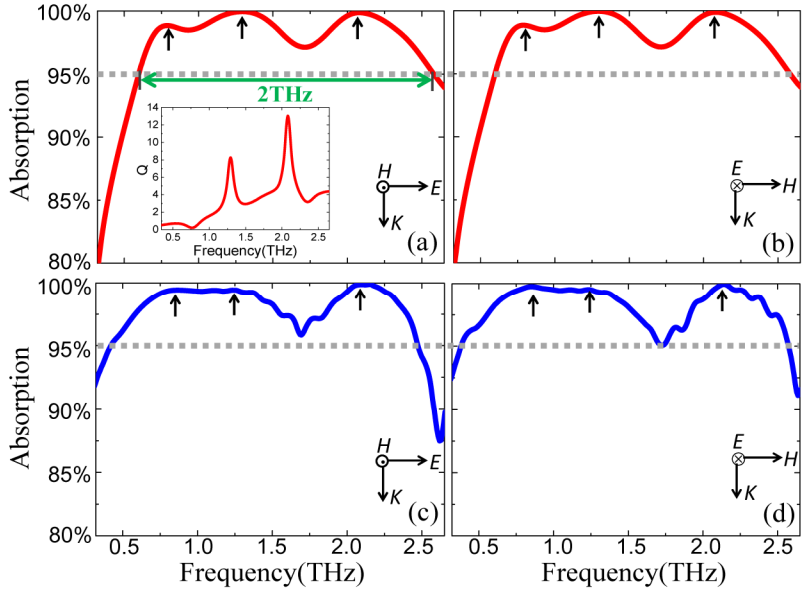

Fig. 2. Calculated ((a), (b)) and measured ((c), (d)) absorption spectra of the THz absorber. (a) and (c) for TE incident THz wave, (b) and (d) for TM incident THz wave. The inset in (a) is the corresponding quality factor of the THz absorber.

We analyze the mechanism of these three peaks nearly at $f = 0.789$ THz, $f = 1.294$ THz, and $f = 2.083$ THz, respectively. The calculated absorption spectra of the double-layered array, with $h_1 = h_2 = 40\mu$m, together with single-layered arrays with $h_1 = 40\mu$m and $h_2 = 40\mu$m are plotted in Fig. 3(a). The broadband absorption [see the red line in Fig. 3(a)] of the double-layered array can be considered as the absorption superposition of these two single-layered arrays, as shown in Fig. 3(a) by blue and yellow lines. For $f = 0.789$ THz, by comparing the red and blue line in Fig. 3(a), the double-layered grating resonance frequency is nearly overlapped with the single-layered grating with width of 80 μm, which demonstrate that the left absorption peak of the double-layered array structure is mainly attributed to the bottom grating array. The corresponding field distributions of both the double-layered and the single-layered array are depicted in Figs. 3(b) and 3(c), respectively. For the double-layered structure, the electric field is mainly located in the air gap between the bottom grating array. This also verifies that the left peak at $f = 0.789$ THz is caused by the air gap in the bottom grating array, which can be considered as local air gap resonance mode. In this case, the incident THz wave is transmitted into substrate and the grating structure [see the electric field

#226580 - $15.00 USD Received 10 Nov 2014; revised 1 Jan 2015; accepted 20 Jan 2015; published 26 Jan 2015

distribution of Fig. 3(b)]. Hence, the incident energy is dissipated in substrate and the grating structure. In addition, the left absorption peak of the double-layered grating array appears red shift as comparing with the case of the single-layered grating [by comparing the red line (0.789 THz) and the blue line (0.858 THz) in Fig. 3(a)]. Here, this small red shift can be explained qualitatively as follows: although most of the incident THz wave at 0.789 THz is trapped in the air gap of the bottom grating array, the impact of the upper grating array cannot be completely ignored. As shown in Fig. 3(b), the incident THz wave is mainly captured in the bottom air gap, and meanwhile a small fraction of THz wave is located in the interface between the upper and bottom grating array [see the field distribution in elliptic region of Fig. 3(b)]. In Fig. 3(d), we can see that although there is no air gap resonance mode in the upper single-layered grating array at 0.789 THz, part of the incident THz wave energy is still gathered in the interface between the grating and the substrate [see the field distribution in elliptic region of Fig. 3(d)]. Therefore, this part of incident THz wave located in the interface between the upper and the bottom grating is determined by the upper grating array. Meanwhile, the trapped field located in interface couples with the air-gap resonance mode (in the bottom grating), and thus the bulk resonance frequency (the left resonance peak in double-layered grating array) is modulated by the interaction between the located field (in interface between the upper and bottom grating) and the air-gap resonance mode, resulting in the red shift of the first resonance frequency in the double-layered grating array.

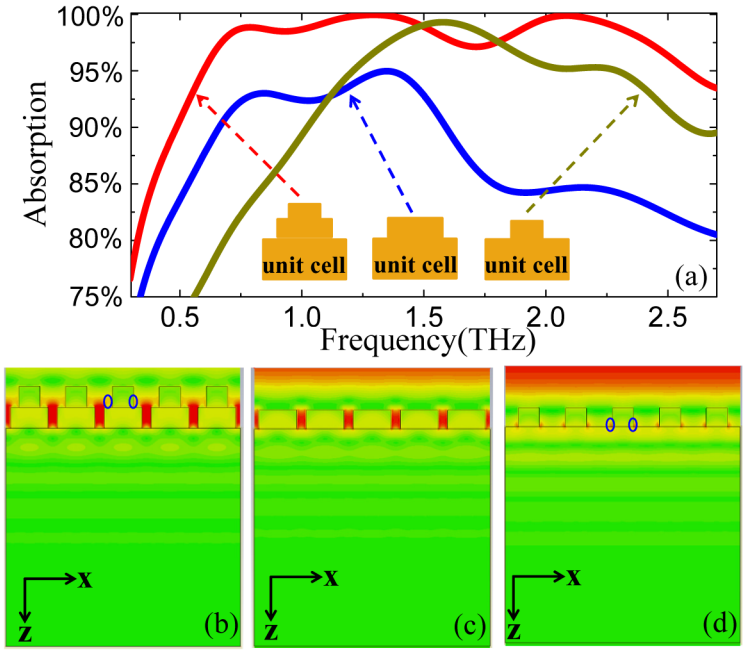

Fig. 3. (a) The calculated absorption spectra of the double layered grating array (red line) and the single-layered grating array with width of 80 μm (blue line) and 45 μm (yellow line). (b), (c), and (d)The field distributions of the double layered grating array (a) and the single-layered array with width of 80 μm (c) and 45μm (d) at 0.789 THz, respectively.

Furthermore, there are another two peaks at f = 1.294 THz, and f = 2.083 THz, as shown in Fig. 3(a). In this frequency range (1.0~3.0 THz), the period of the structure is larger than the wavelength in the doped-silicon but still smaller than that in free space ($\lambda/n<p<\lambda$) [26]. Thereby, in this case, the air gaps between the double-layered grating arrays can be considered as waveguides to diffract THz wave into the substrate. In Fig. 4(a), based on two-dimensional rigorous coupled-wave analysis (2D-RCWA) method, we calculate the grating diffraction of this double-layered grating structure. These two peaks at f = 1.294 THz, and f =

#226580 - $15.00 USD Received 10 Nov 2014; revised 1 Jan 2015; accepted 20 Jan 2015; published 26 Jan 2015

2.083 THz are mainly resulting from the [± 1, 0]-order and [± 2, 0]-order grating diffractions, respectively, as shown in Fig. 4(a). Here, we want to emphasis that although the two peaks at 1.294 THz and 2.083 THz are mainly attributed to the first and second grating diffractions, respectively, other orders of grating diffraction cannot be ignored completely. For example, at 2.083 THz, the resonance peak is the combined effect of the zero-order, first-order, and second-order grating diffraction (in which the second-order grating diffraction has the most obvious effect). Figures 4(b) and 4(c) show the corresponding field distributions of these two peaks, and we can see that some energy is transmitted into the substrate through the air gap [labeled by the arrows in Figs. 4(b) and 4(c)]. The residual energy is consumed in the process of the grating diffractions in the double-layered grating. Therefore, by choosing the properly geometrical parameters of the double-layered grating structure, the [± 1, 0]-order and [± 2, 0]-order grating diffractions and the air gap mode resonance can be combined to form an ultra-broadband THz absorber.

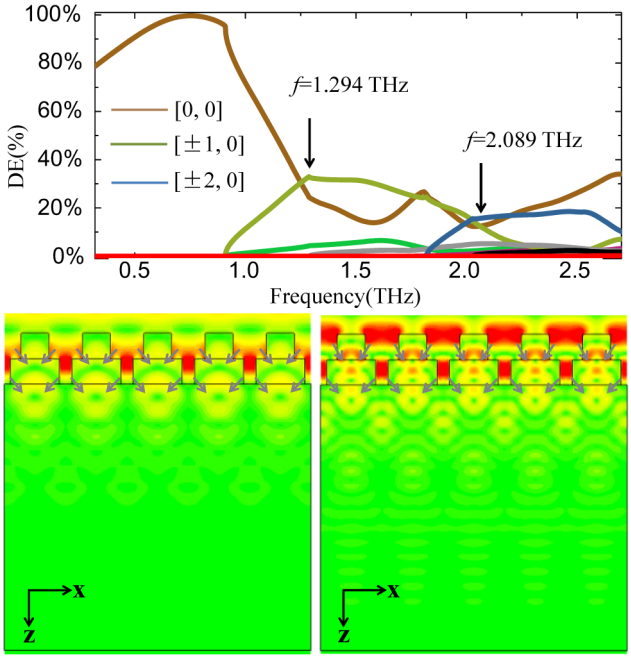

Fig. 4. (a) The diffraction efficiency (DE) of different diffraction orders. (b) and (c) The field distributions of the double layered grating array at 1.294 THz and 2.083 THz, respectively.

As practical applications, for non-normal incident radiation, the absorption at different incidence angles for TE and TM polarizations are illustrated in Fig. 5. For TE incident THz wave, as presented in Fig. 5(a), the absorption efficiency is above 95% with bandwidth 2 THz for oblique angle as large as 45°. For TM incident THz wave, although the oblique angle is larger than 55°, the absorption efficiency is still above 95% with bandwidth 2 THz. Therefore, this kind of broadband THz absorber can work in a large oblique incident angle.

#226580 - $15.00 USD Received 10 Nov 2014; revised 1 Jan 2015; accepted 20 Jan 2015; published 26 Jan 2015

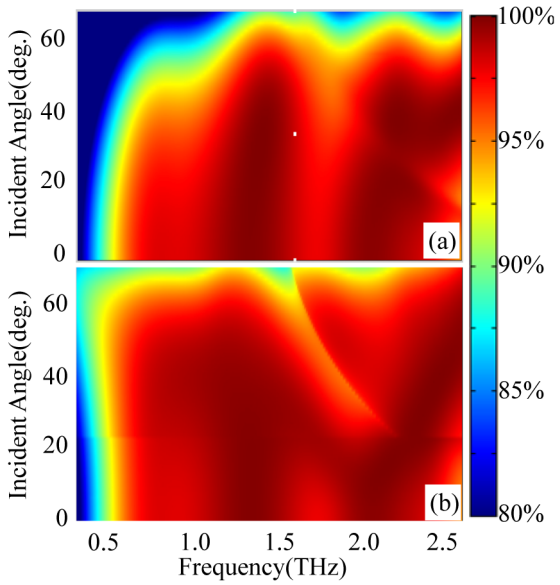

Fig. 5. The absorption spectra with different incidence angles for (a)TE polarized THz wave, and (b)TM polarized THz wave.

3. Conclusion

In summary, we have proposed a double-layered grating structure to realize an ultra-broadband polarization-independent THz absorber by combing the air-gap mode resonance, the first- and second-order grating diffractions. The double-layered grating structure can be fabricated on the surface of the doped silicon by using the ICP etching. The measured results demonstrate that the incident THz waves can be 95% absorbed with a bandwidth over 2 THz. Both the theoretical simulations and the experimental results agree well with each other. Such an ultra-broadband THz absorber may be applied into THz imaging system, anti-radar cloaking, sensor and so on.

Acknowledgments

This work is partly supported by the National Program of Key Basic Research Project of China (973 Program, 2014CB339806), Major National Development Project of Scientific Instrument and Equipment (2011YQ150021, 2012YQ14000504), National Natural Science Foundation of China (11104186, 61307126, 61138001), the Scientific Research Innovation Project of Shanghai Municipal Education Commission (14YZ093), the Key Scientific and Technological Project of Science and Technology Commission of Shanghai Municipality (12JC1407100), the Program of Shanghai Subject Chief Scientist (14XD1403000).

#226580 - $15.00 USD Received 10 Nov 2014; revised 1 Jan 2015; accepted 20 Jan 2015; published 26 Jan 2015